

PARAMETRIC ANALYSIS OF MANUFACTURING COMPOSITE STRUTS WITH AUTOMATED FIBER PLACEMENT

Alex Brasington¹, Matthew Godbold¹, Ramy Harik¹

¹University of South Carolina
McNAIR Aerospace Center, Department of Mechanical Engineering
1000 Catawba Street
Columbia, SC 29201

ABSTRACT

Automated fiber placement (AFP) manufacturing with carbon fiber composites is becoming increasingly popular in manufacturing sectors. Since its inception, this technique has been mainly used for simple geometries; however, research has led to the possibility of increasingly complex structures. One such type of complex geometry to be investigated is a strut. Struts are largely seen in structures such as lunar landers and aircraft. The layout of such a complex geometry produces defects that can hinder the structural performance of the final part. This report investigates the manufacturability of such a geometry by investigating the geometry and path planning combined with a tool to rapidly iterate on the design variables. The result is a strut geometry optimal for limiting defects with predicted manufacturability scores displaying potential issues that could be seen in the manufacturing process.

Keywords: Automated Fiber Placement, Design for Manufacturing, Struts

Corresponding author: Ramy Harik (harik@mailbox.sc.edu)

1. INTRODUCTION

Struts are omnipresent in deployable parts of aircraft and spacecraft. This includes supports for solar panels, lunar lander struts, lunar surface components, strut-based wing components, aircraft spars, or unmanned aerial vehicles [1]. For lunar landers such as the Human Landing System shown in Figure 1, composites are under consideration to reduce weight of the structure. Unlike general applications of struts, lunar lander struts require greater strength requirements due to high compression load during launch and ascent [1].



Figure 1: Human Landing System [2]

A typical strut geometry is presented in Figure 2 consisting of a main body, tapered section, and fitting region. Jegley et al. presents investigations into the efficiency of utilizing composite struts for aerospace applications [1].

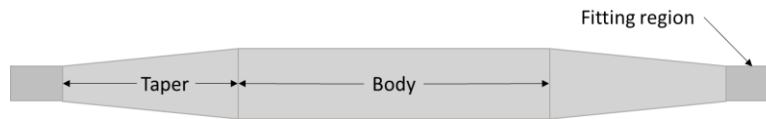


Figure 2: Diagram of a typical strut geometry

In these studies, Lockheed Martin [3], Boeing [4], and Northrop Grumman [5] presented their analysis on the optimum design. A series of strut sizes and stacking sequences were used. The strut geometries varied greatly with various total lengths, untapered lengths, taper angles, and fitting lengths. To provide a general understanding of the strut sizes, Table 1 presents the geometry variations. It was concluded that the carbon-epoxy tapered struts provide a lighter weight alternative to aluminum-lithium alloys for aircraft or spacecraft structures. The geometry still requires an efficient method for manufacturing. Hand layup is a common option for complex geometries, though this is not scalable if a multitude of parts are necessary. For this purpose, the use of Automated Fiber Placement (AFP) is investigated.

Table 1: Description of the strut geometries investigated in

Strut Length (in)	Central Diameter (in)	Untapered Length (in)	Taper Angle (°)	Fitting Length (in)
60.9	2.5	42.5	4	2.04
100.3	2.0	92.7	10	1.25
77.7	6.0	50.7	10	2.94
127.0	6.0	73.7	4	2.94

AFP is a composite manufacturing technique developed about 30 years ago. This technique utilizes a gantry or robotic system with an attached fiber placement head that enables multiple strips, or tows, to be laid onto a tool surface. AFP has been consistently evolving, manufacturing composite parts with higher speed, repeatability, and improved quality. Flat, low curvature geometries, and

cylinders have been the primary areas of research, but AFP is now being used on parts with increasing complexity. This study aims to investigate the manufacturability of landing struts for lunar landers through AFP. Moreover, AFP is also explored for the manufacturing of small and medium parts, versus the traditional large structures. Previously complex parts had to be manufactured through manual lay-up which is a costly and time-consuming process – as well as having accuracy issues – where each composite layer is placed by hand. Although such a process allows for a wider range of applicable surface complexity, it is costly and is not feasible for increased throughput therefore the adaptation of the AFP process is beneficial.

A strut holds several barriers for AFP, one major issue is the geometry of the strut. The strut geometry is unique in that it consists of two different constant radius cylinders connected via a transition zone. This transition zone can be linear or radial and can vary in length as well as the two existing diameters. Dimensional requirements will be based on structural performance and layup quality as found in this study. Layup of complex geometries such as a strut, is a common difficulty in AFP manufacturing due to tow steering which can increase defect formation [6], [7]. Manufacturing with such limited space can be problematic and introduce large amounts of fiber defects, including gaps, overlaps, angle deviation, and steering [8], [9]. These manufacturing defects can lead to decreased performance of composite laminates and failure characteristics over time due to increased fatigue [10], [11]. The initial investigations of manufacturability will be conducted using MATLAB [12], while the final tool will be developed with Python [13].

2. ALGORITHMS AND DESIGN TOOL

Design and optimization are highly effective in minimizing the defects in AFP layup especially on complex geometries [14], [15], [16], therefore, significant work was done in this area. Two transition zones are considered for analysis, linear and radial. The transition zone is created with the variables presented in Figure 3. Note that the linear transition is obtained with zero values for R_1 and R_2 . When developing the algorithm, several aspects of composite manufacturing had to be considered. Seven standard manufacturing angles were considered from zero degrees to ninety degrees (0° , 15° , 30° , 45° , 60° , 75° , 90°). For defect optimization, four types of defects were considered: angle deviation, gaps, overlaps, and steering.

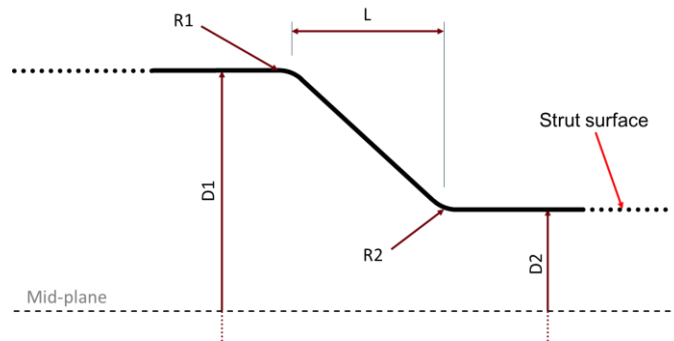


Figure 3: Diagram of the strut transition geometries with the design variables labeled

2.1 Transition Zone Algorithm

The initial analysis consists of investigating the transition zone of the strut, highlighted below in Figure 4. It is known that this zone will cause the most issues during manufacturing, therefore optimizing the geometry in this location is a beneficial starting point. Each of the variables used in the derivation of the algorithm are also labeled in Figure 4. Here, D_1 and D_2 represent the larger and smaller diameters respectively, L is the total length of the transition zone, S is the 2D change in the two diameters, F is the length of the sloped portion of the transition zone, and α is the angle of the slope. The derivation of the algorithm to be used is presented below.

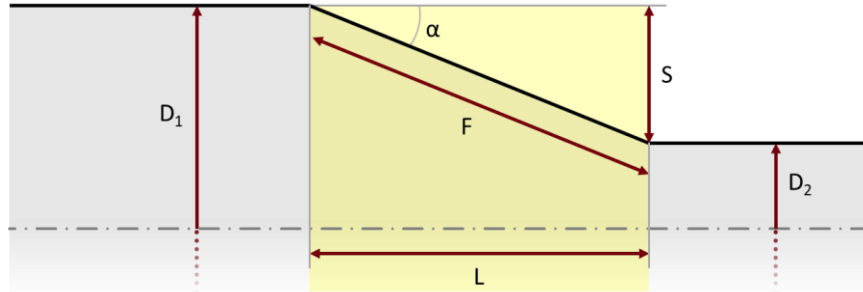


Figure 4: Diagram of strut geometry with defined variables

The first item to consider when analyzing the transition zone is the difference between the two diameters that are being connected (S). This difference is found through Equation 1. In this equation the difference in the diameters is divided by 2 to arrive at the difference for only one side of a 2D projection of the struts surface.

$$S = \frac{D_1 - D_2}{2} \quad 1$$

The next critical aspect of the geometry is the slope of the transition zone as this will determine how quickly the diameters will change. The angle (α) is calculated from Equation 2 below. This equation considers S found above along with the total transition length (L).

$$\alpha = \tan^{-1}\left(\frac{S}{L}\right) \quad 2$$

With α calculated, the total diameter loss around strut per course (dT) can be found with Equation 3. This value provides the change in diameter at the end of the last tow in each course. The dT value will be used in the final ratio calculation to determine manufacturability of the transition zone in question.

$$dT = 2\pi * t * w * \sin(\alpha) \quad 3$$

Next, using the transition angle and the known transition length, the length of the sloped portion of the transition zone, termed fiber slope (F), can be found with Equation 4.

$$F = \frac{L}{\cos\alpha} \quad 4$$

The fiber slope, number of tows per courses (t), and the width of each tow (w) are now used to determine the number of courses (n) that are needed to cover the transition area with Equation 5. Note that the n value to be used is the maximum number of courses that can fit within the transition zone, and this happens when the fiber angle is 90-degrees assuming 0-degrees is along the length of the strut. For the case of this algorithm, this will be the worst-case scenario since the maximum number of tows will be within the transition zone. Also note that it is not assumed that the 90-degree ply will be the most difficult one, it only provides the most tows within the transition zone.

$$n = \frac{F}{t * w} \quad 5$$

To obtain the actual number of courses needed (r), the n value is rounded up to the next whole number. The diameter loss of the current course (DL_i) is then calculated with Equation 6. In this equation, n_i represents the current course number with the first course beginning at the largest diameter and progressing towards the smallest.

$$DL_i = \left(\frac{n_i}{r}\right) * (D_1 - D_2) \quad 6$$

Utilizing the local diameter loss, the standardized diameter loss per course (SDL_i) with respect to the initial diameter can be obtained with Equation 7. This value provides the current diameter with respect to the diameter that has been lost at the current course.

$$SDL_i = D_1 - DL_i \quad 7$$

Finally, the ratio for each course ($Ratio_i$) is found by dividing dT by the new perimeter and multiplying by 100 (Equation 8). A lower ratio value represents a better result for the current course. It should be noted that this algorithm does not include effects of radii at the beginning and end of the transition zone. However, due to the small radii used in experimentation, this method can still be used to approximate the effect of the transition zone length and the number of tows.

$$Ratio_i = \frac{dT}{2\pi * SDL_i} * 100 \quad 8$$

To further understand what this output represents, the following graphs present example results with given diameters and transition length values. Figure 5 displays the effect of modifying the transition length of the strut. It becomes obvious that as the transition length decreases, the ratios increase drastically. However, there is a point where further increase of the transition length leads to diminishing returns.

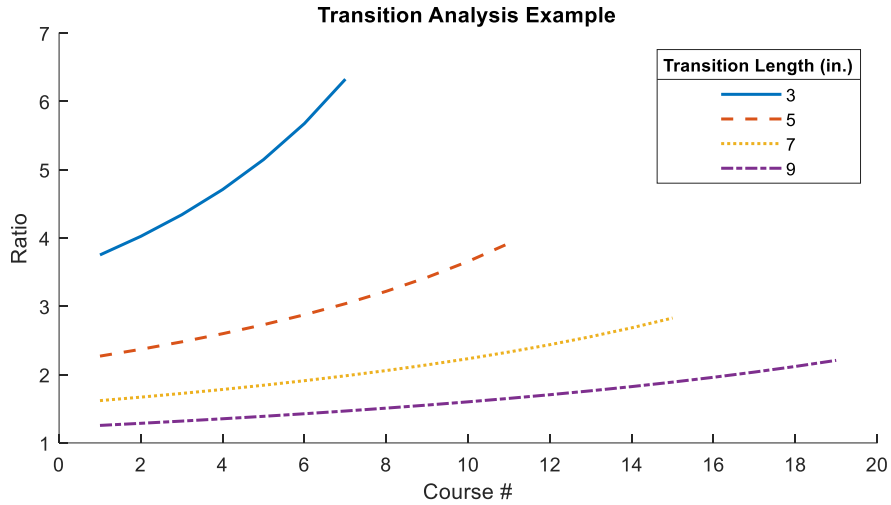


Figure 5: Plot of ratio values for various transition lengths

From the equations presented above, it is clear that the ratio is highly dependent on the transition, and the transition zone is a function of S and L. To analyze each transition length, the integral of each curve from Figure 5 is computed. This integral is approximated by summing the ratio values at each course and is then divided by the total number of courses (r), as presented in Equation 9.

$$\sum_{i=1}^r \text{Ratio}_i / r \tag{9}$$

Performing this calculation at various S and L values results in the plot shown in Figure 6. As previously stated, the ratio values initially change drastically with the transition length. This plot also shows that as the S value decreases, the ratios also decrease. A lower S value would mean that the two diameters are closer each other. This value is usually set based on the structural requirements; therefore, more emphasis should be given to the transition length.

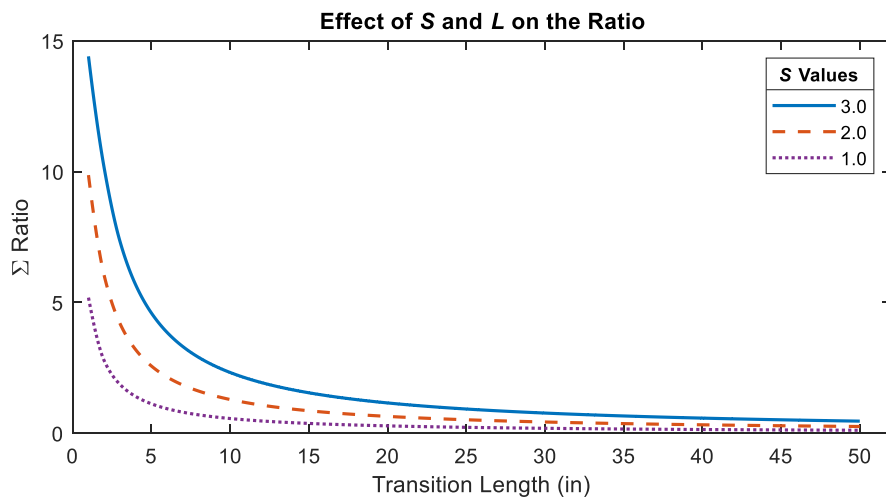


Figure 6: Plot showing the effect of variables S and L on the ratios

Lastly, the number of tows per course will also affect the ratios due to its role in Equation 6. Figure 7 presents this effect graphically with the number of tows varying for 2 to 4 per course. It is immediately seen that decreasing the number of tows per course improves each of the ratio values. This factor can be utilized to determine what the optimal course width is when combined with the defect output.

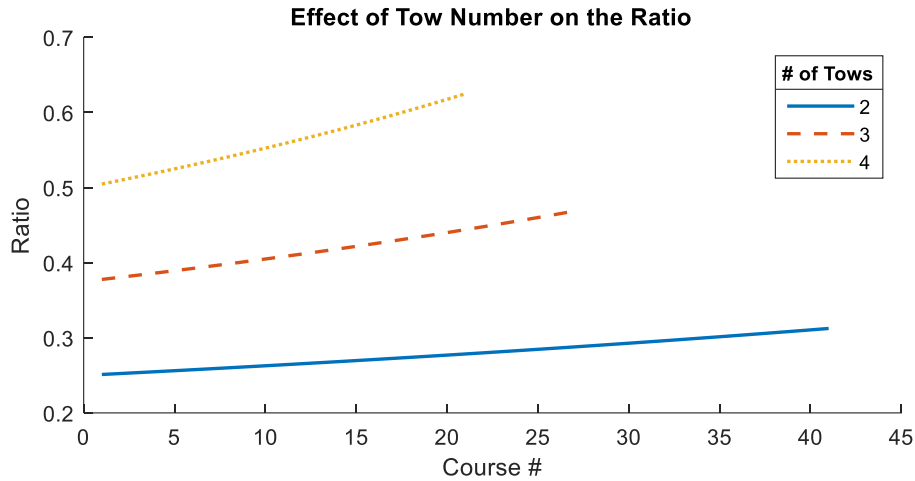


Figure 7: Plot showing the effect of tows per course on the ratio

The presented algorithm provides an initial assessment of the transition zone along with trends related to changing the various variables relating to the transition zone. This method presents limitation when AFP defects are considered as it does not factor in any defects with the courses. With AFP defects being a large part of the structural and manufacturing performance, they must be considered. To tackle this limitation, the Computer Aided Process Planning (CAPP) software is used to evaluate defect occurrence and severity. The software functionalities are described below.

2.2 CAPP Algorithm

The CAPP [17] process leverages the well-developed VERICUT Composites Programming (VCP) [18] functionalities. The process begins with splitting the tool surface at each ply boundary to isolate the surface inside (Figure 8a). The inner surface is then meshed with a user specified density. Using the mesh surface, a heat kernel signature (HKS) analysis is performed (Figure 8b). This calculation basically heats up the part and sees where the heat is last to dissipate from. Each of these processes are classified as surface preparation for subsequent processing.

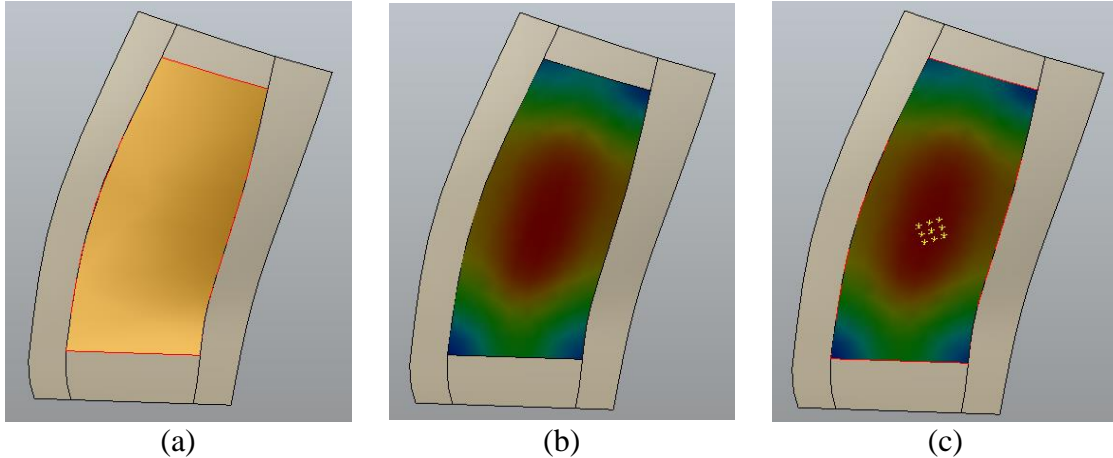


Figure 8: Example of the steps of the CAPP process: (a) surface splitting, (b) HKS calculation, (c) starting point creation

Next, the user can select an option to build the starting point arrays. Before building scenarios, the user can select which layup strategies to use from those available in VCP (Figure 9). A scenario will be built for each strategy selected.

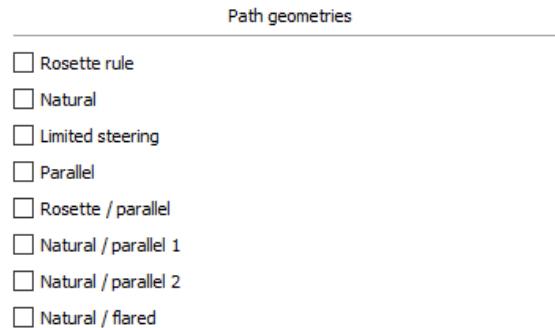


Figure 9: User selection of layup strategies

The user can either build a single starting point for each strategy at the max HKS value or build a 3x3 matrix for each with the center point at the max HKS value (Figure 8c). Building a single scenario is used for rapid analysis of manufacturability, whereas the matrix of points is utilized for optimization of the starting point. The last option is to build another 3x3 array of points centered on the best scenario extracted through the scoring process. This iteration process can be done until a point is converged on, or until the user is satisfied the manufacturability score.

The generated scenarios can then be exported to a template that can be imported directly into VCP. With the imported data, VCP generates the courses and provides an anticipated defect analysis. This analysis contains data associated with gap, overlap, angle deviation, and steering defects. The data generated by VCP is then imported back into the CAPP environment and is visually available through the CAD viewer and through histograms (Figure 10).

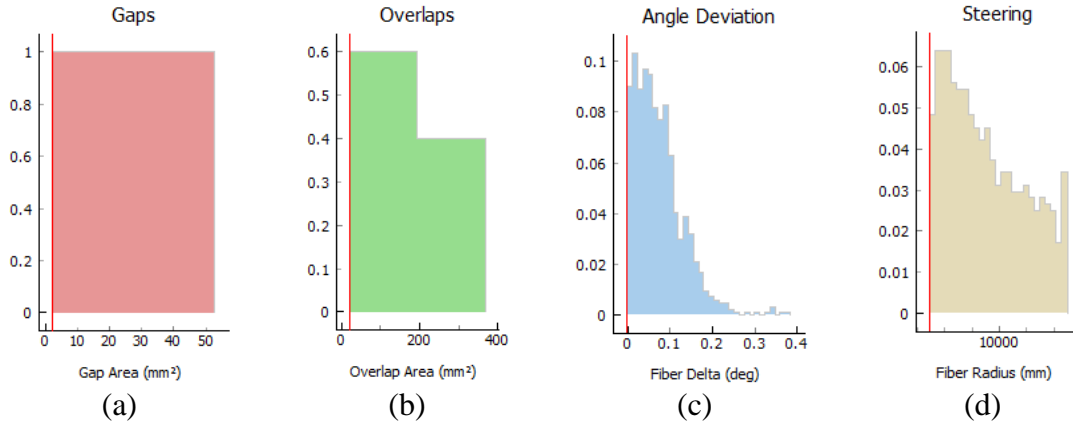


Figure 10: Histogram representation of (a) gaps, (b) overlaps, (c) angle deviation, and (d) steering defects

In order to analyze the imported defect data, the user must first input some values. The first values to input are threshold values for gap area, overlap area, angle deviation allowance, and steering radius allowance. The input values can then be used to compute instances and severity of each defect using the Equation 10 and 11 below.

$$Instance = \frac{\# Unacceptable}{\# Total} \quad 10$$

$$Severity = \frac{Accumulated\ defect\ above\ threshold}{Total\ sum\ of\ defects} \quad 11$$


The results are then tabulated and presented within the software as shown in Figure 11. An instance and severity value of 1 corresponds to all the defects being above the acceptability limit given by the user.

Feature Threshold Values			
	Threshold	Instance	Severity
Gap	25.4 mm ²	0.50	0.83
Overlap	25.4 mm ²	0.92	1.00
Angle Dev.	2.0 deg	0.06	0.26
Steering	2×10 ³ mm	0.32	0.55

Figure 11: Feature threshold chart

To calculate a single score that combines instance and severity of each defect, an analytic hierarchy process (AHP) matrix is used (Figure 12). The goal of this matrix is to rank each set of defects based on their importance. The user can change the values within the AHP matrix to put priority on certain defects. This matrix is then converted into rankings that are used to compute the score of each scenario.

	Gap Instances	Gap Severity	Overlap Instances	Overlap Severity	Angle Dev. Instances	Angle Dev. Severity	Steering Instances	Steering Severity
Gap Instances	1.0	1.0	1.0	1.0	1.0	1.0	1.0	1.0
Gap Severity	1.0	1.0	1.0	1.0	1.0	1.0	1.0	1.0
Overlap Instances	1.0	1.0	1.0	1.0	1.0	1.0	1.0	1.0
Overlap Severity	1.0	1.0	1.0	1.0	1.0	1.0	1.0	1.0
Angle Dev. Instances	1.0	1.0	1.0	1.0	1.0	1.0	1.0	1.0
Angle Dev. Severity	1.0	1.0	1.0	1.0	1.0	1.0	1.0	1.0
Steering Instances	1.0	1.0	1.0	1.0	1.0	1.0	1.0	1.0
Steering Severity	1.0	1.0	1.0	1.0	1.0	1.0	1.0	1.0



	Rankings
Gap Instances	0.12
Gap Severity	0.12
Overlap Instances	0.12
Overlap Severity	0.12
Angle Deviation Instances	0.12
Angle Deviation Severity	0.12
Steering Instances	0.12
Steering Severity	0.12

Figure 12: AHP matrix and rankings

The individual scenario scores are computed using Equation 12. Here the ranking weights are those computed through the AHP matrix, and the measurement values are from the instance and severity calculations. The scores for all scenarios can be automatically computed with the manufacturability button. This also finds the best score for each ply and stores it for further manufacturability calculations.

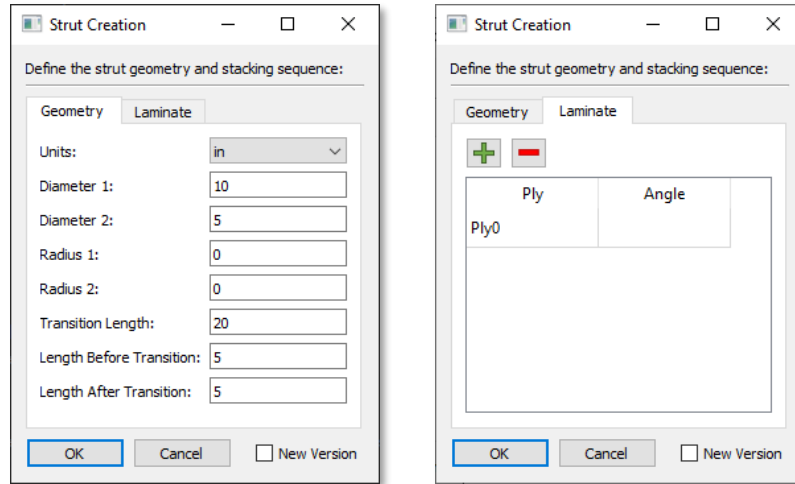
$$Score = \sum Ranking\ Weight * Measurement\ Value \quad 12$$

The final manufacturability calculation for the entire laminate is computed using Equation 13. In this equation, the score is the maximum score from all scenarios in the associated ply. The ply area represents the surface area within the appropriate ply boundary. This equation allows for the total manufacturability to be a function of the size of each ply. Therefore, a smaller ply affects the score less than a larger one. A manufacturability score of 1 is the best possible value, while 0 is the worst. Through future manufacturing trials, a threshold manufacturability value will be found to define if it is acceptable to continue with manufacturing or if further refinement is necessary.

$$Manufacturability = \sum_{n=1}^{\#plies} Score_n * Ply\ Area_n / \sum_{m=1}^{\#plies} Ply\ Area_m \quad 13$$

2.3 Design Tool

To provide a rapid iteration capability a design tool was developed to directly build a strut, perform the transition zone analysis, and pass the geometry to the CAPP software. This application was built in Python and provides the user a dialog with input options to define the shape of the strut and the stacking sequence. Figure 13a provides an image of the user input options which includes the variables from Figure 2.1 and options for distances before and after the transition. Figure 13b shows the definition of the stacking sequence where the user can add and remove plies and set the ply angles.



(a)

(b)

Figure 13: User dialogs for creating strut surface and stacking sequence

Creation of the actual geometry is performed with a Python wrapper of Open Cascade (PythonOCC) [19]. This platform allows a programmatic approach to creating CAD entities utilizing the open-source functionalities of PythonOCC. Using the design inputs, a strut profile is created that defines the 2D representation of the outer shape. This profile is then revolved around a central axis to create the strut's surface. The two circles that are created from the diameter inputs are then projected and offset by a defined amount to form the ply boundary. For the case of these experiments only a single ply boundary is utilized for every ply angle. The creation of the strut is summarized graphically below in Figure 14.

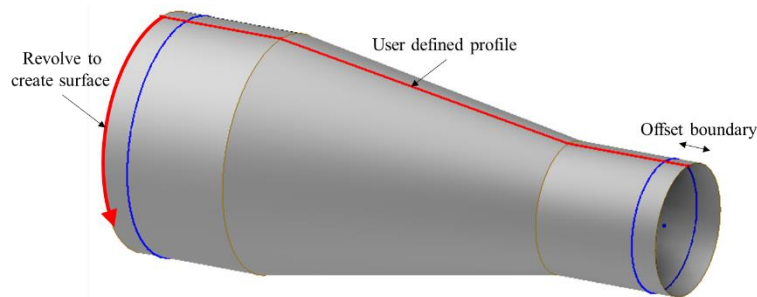


Figure 14: Graphical description of how the strut surface and boundaries are created

An example geometry output is shown below in Figure 15. This geometry is then analyzed by the transition zone algorithm and passed to the CAPP process. Once analysis is done on this version of the strut, a new one can be created in the same way. All analysis can then be compared directly to determine the best geometry.

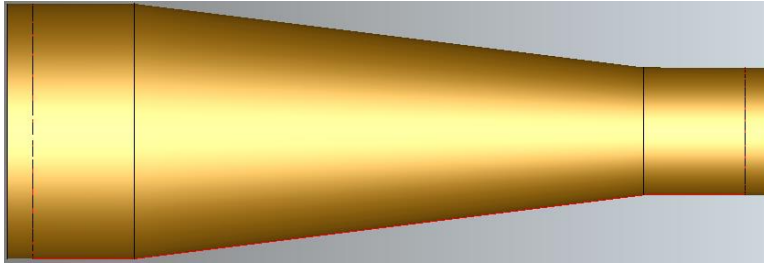


Figure 15: CAD output of the design tool

3. EXPERIMENTATION PLAN

3.1 Test Matrix

Experimentation consisted of a parametric study of a general strut geometry to investigate its manufacturability based on various design inputs and to choose an optimal shape. The design parameters are set to be the transitions length and the radius at the beginning and end of the transition zone. Three different transition zone lengths (7 in., 14 in., 22 in.) and three radii values (0 in., 1 in., 2 in.) are used resulting in the 9 design variations shown in Figure 16.

	L = 7 in	L = 14 in	L = 22 in
R = 0 in			
R = 1 in			
R = 2 in			

Figure 16: Graphical representation of the strut trial test matrix

The trial IDs that will be used to differentiate between each trial are presented in Table 2. For each ID, the first number represents the trial number, and the second number represents the number of tows used in the respective trial. This table also provides each of the design variables used for each trial. All trials utilized tows with a width of 0.25 in. Also note that all trials use the rosette rule layup strategy due to unsuccessful course generation with other strategies in VCP.

Table 2: Description of each variable for the various trials

Trial	D1 (in.)	D2 (in.)	L (in.)	R1 (in.)	R2 (in.)
1-4	4.75	2.75	7	0	0
2-4	4.75	2.75	14	0	0
3-4	4.75	2.75	22	0	0
4-4	4.75	2.75	7	1	1
5-4	4.75	2.75	14	1	1
6-4	4.75	2.75	22	1	1
7-4	4.75	2.75	7	2	2
8-4	4.75	2.75	14	2	2
9-4	4.75	2.75	22	2	2
1-2	4.75	2.75	7	0	0
2-2	4.75	2.75	14	0	0
3-2	4.75	2.75	22	0	0
4-2	4.75	2.75	7	1	1
5-2	4.75	2.75	14	1	1
6-2	4.75	2.75	22	1	1
7-2	4.75	2.75	7	2	2
8-2	4.75	2.75	14	2	2
9-2	4.75	2.75	22	2	2

*Rosette Rule used; other strategies generated errors in VCP

3.2 CAPP Ranking Strategy

As mentioned in Section 2.2, the manufacturability scoring is highly dependent on user inputs for the threshold of each defect and AHP matrix values. For the presented experiments, the gap and overlap thresholds are set to 25.4 mm², the angle deviation threshold is set at 2 deg, and the steering threshold is set at 2000 mm. The values chosen are typical values that are of concern for each defect. Below the given values, it is assumed that the defects will have a small effect on the structural performance. The threshold values are summarized below in Table 3.

Table 3: Defect threshold values for the experiments

Defect	Threshold Value
Gap	25.4 mm ²
Overlap	25.4 mm ²
Angle Deviation	2 deg
Steering	2000 mm

For the AHP matrix, all values are chosen to be 1. This will factor in each defect's instance and severity equally, leading to a scoring that incorporates all defects. All defects are to be factored

equally to create a broad overview of possible issues with each investigated design. The overall rankings generated from the AHP matrix are provided in Table 4.

Table 4: AHP ranking for each defect category

Item	Ranking
Gap Instances	0.12
Gap Severity	0.12
Overlap Instance	0.12
Overlap Severity	0.12
Angle Deviation Instances	0.12
Angle Deviation Severity	0.12
Steering Instances	0.12
Steering Severity	0.12

4. RESULTS AND DISCUSSION

4.1 Transition Zone Analysis

The results of the transition zone analysis for 4 tows and 2 tows are presented below in Figure 17a and Figure 17b respectively. Both plots show that as the transition length increases, the ratio decreases. This represents a better predicted manufacturability as the transition length increases. It can also be seen that 2 tows are predicted to outperform 4 tows for each transition length. This is attributed to each course having to cover less of a differential in diameter when using 2 tows instead of 4.

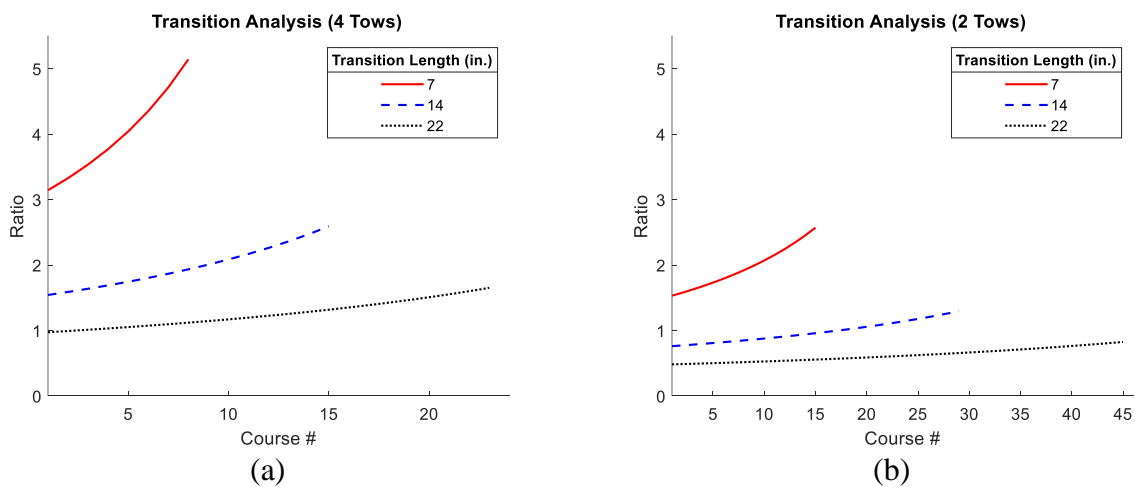


Figure 17: Transition zone analysis with (a) 4 tows and (b) 2 tows

Further examination of using 4 tows versus 2 tows was performed with the results shown in Figure 18. Again, it is seen that 2 tow trials are predicted to perform better at every transition length. This

figure also provides some insight into how the ratios change as a function of transition length. A quick improvement is seen with initial increases in transition length with depreciating results with changes in longer transition lengths.

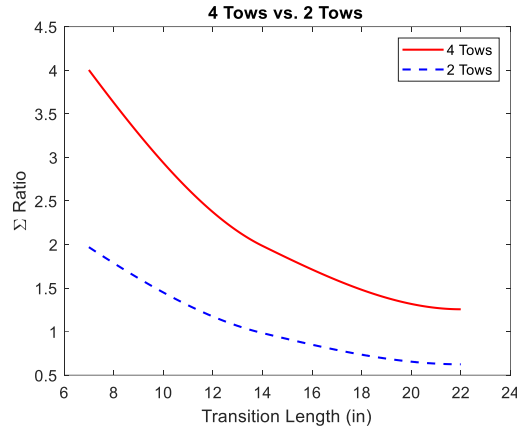


Figure 18: Direct comparison of manufacturing with 2 and 4 tows

4.2 Defect Analysis

The overall manufacturability results for the 4 tow trials are shown below in Figure 19. Each bar represents a ply’s score, while the data points show the combined laminate score. Note that the 90-degree plies are not included due to no defects being present for both the 4 tow and 2 tow trials. Initial observation of the figure shows little variation between each of the trials with slight increases in laminate scores as the transition length increases.

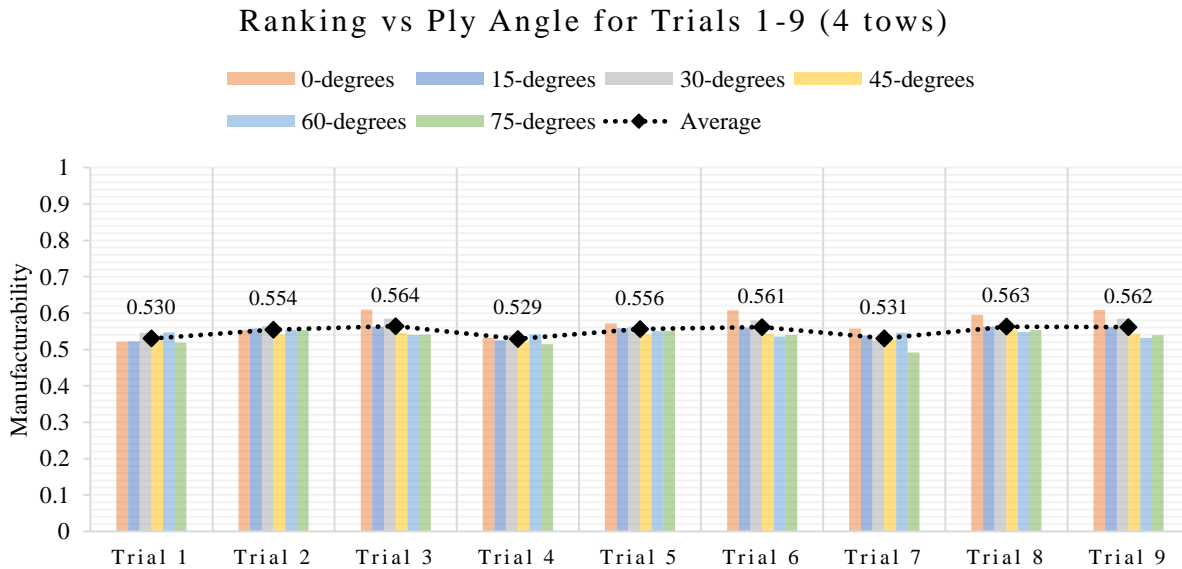


Figure 19: Ply and laminate scores for each trial with 4 tows

The scores of each of the ply angles presented above are summarized in Table 5. These values are averages of the 9 trials for each angle. For the 4-tow case, the 0-degree plies performed best while the 75-degree plies performed the worst. The low scores of the 75-degree ply are attributed to an increase in defects seen in the transition zone.

Table 5: Average ply scores for the 4 tow trials

Ply Angle	Rank
0	0.573
15	0.550
30	0.561
45	0.538
60	0.544
75	0.534
*4 tows	

Similarly, the laminate average scores are presented in Table 4.2. For each radius value used, the shortest transition lengths performed the worst, while the longest transition lengths performed the best. However, the variation in scores is small and is nearly negligible.

Table 6: Average laminate scores for the 4 tow trials

Trial	Avg. Rank
Trial 1-4	0.530
Trial 2-4	0.554
Trial 3-4	0.564
Trial 4-4	0.529
Trial 5-4	0.556
Trial 6-4	0.561
Trial 7-4	0.531
Trial 8-4	0.563
Trial 9-4	0.562

Figure 20 below is presented to further examine the trends in how the design variables affect the manufacturability. It is seen that increasing the transition length has the largest effect on the manufacturability score. The radius values utilized have little affect regardless of which one is used, and the data is not consistent enough to draw a conclusion.

4 Tow Trial Comparisons

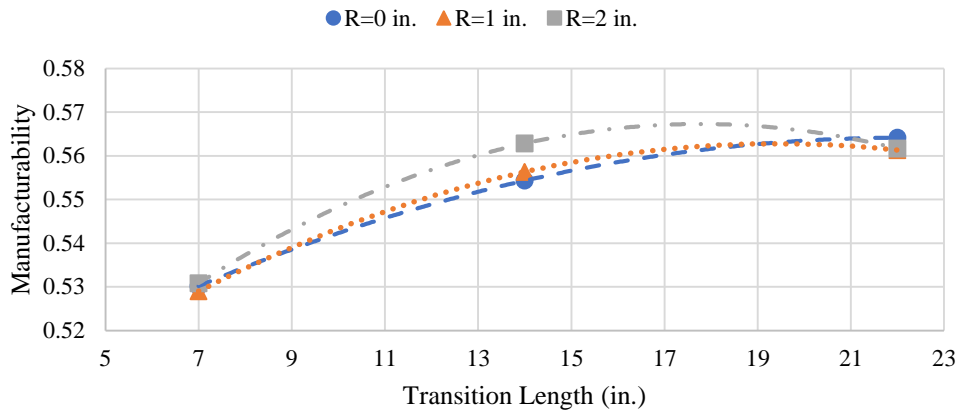


Figure 20: Trends in laminate scores for the 4 tow trials

Similar results are acquired for the 2 tow trials. Figure 21 presents a summary of the results with the ply and laminate scores shown graphically. Immediately it can be seen that all the laminate scores for the 2 tow trials are lower than those seen in the 4 tow trials. The plot also shows a larger differential when increasing the transition length.

Ranking vs Ply Angle for Trials 1-9 (2 tows)

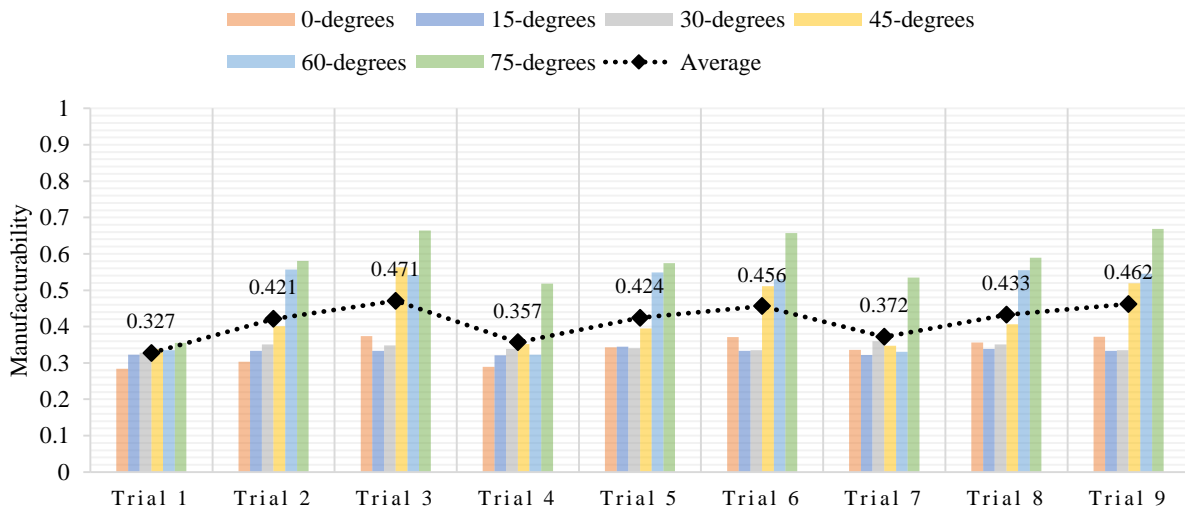


Figure 21: Ply and laminate scores for each trial with 2 tows

The average scores for each ply are presented below in Table 7. Unlike the 4 tow trials, the 75-degree ply has the best score while the 15-degree ply has the worst score. However, the plies as a whole have an overall lower score than the 4 tow trials.

Table 7: Average ply scores for trials with 2 tows

Ply Angle	Rank
0	0.336
15	0.331
30	0.343
45	0.426
60	0.474
75	0.571
*2 tows	

The overall laminate score for each of the 2 tow trials is shown below in Table 8. These values show that a lower transition length produces a lower score while the larger lengths produce a higher score. It can also be seen that there is a larger variation in the laminates with radii values of 0 and 1 than with values of 1 and 2.

Table 8: Average laminate scores for trials with 2 tows

Trial	Avg. Rank
Trial 1-2	0.327
Trial 2-2	0.421
Trial 3-2	0.471
Trial 4-2	0.357
Trial 5-2	0.424
Trial 6-2	0.456
Trial 7-2	0.372
Trial 8-2	0.433
Trial 9-2	0.462

As before, the trends of the 2 tow trials are presented in Figure 22. The results show similar trends when compared with the 4 tow trials. In both cases, increasing the transition length leads to improved overall manufacturability scores. Also, the results from varying radius values are inconclusive with initial increases in manufacturability and the opposite effect with larger transition zones.

2 Tow Trial Comparisons

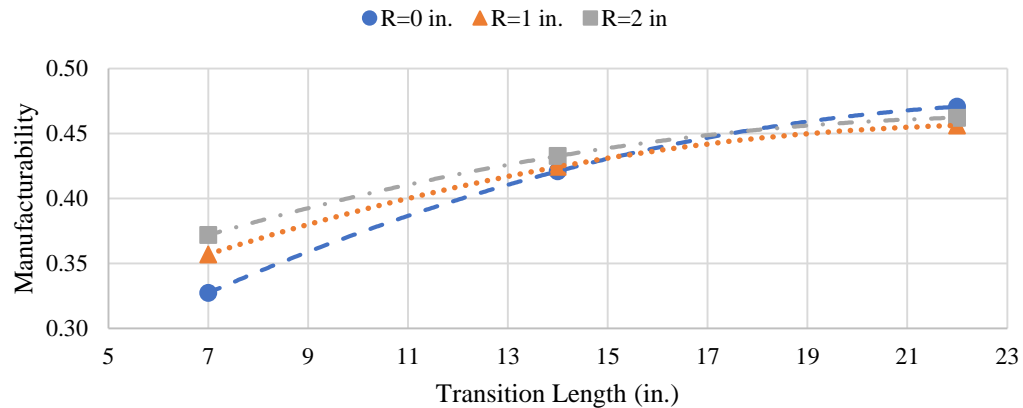


Figure 22: Trends in laminate scores for the 2 tow trials

4.3 Discussion

The laminate scores from the trials presented above are combined and shown in Table 9 below. Again, all the scores from the 4 tow trials are improved when compared with those seen in the 2 tow trials. This increased score is largely due to the defects seen around the transition zone of the strut. Also, VCP checks for defects between courses therefore since more 2 tow courses are required than 4 tow courses, more zones for defects exist. Additionally, increasing the transition zone also improves the overall laminate score.

Table 9: Combined results for trials with 2 and 4 tows

	Trial 1	Trial 2	Trial 3	Trial 4	Trial 5	Trial 6	Trial 7	Trial 8	Trial 9
4 tows	0.530	0.554	0.564	0.529	0.556	0.561	0.531	0.563	0.562
2 tows	0.327	0.421	0.471	0.357	0.424	0.456	0.372	0.433	0.462

Figure 23 below demonstrates the difference in the defects seen in the 4 tow and 2 tow trials with an example analysis of a 45-degree ply. When manufacturing with 4 tows, the individual defect severity may be higher however the instances are significantly higher when manufacturing with 2 tows. In the presented scoring method, this resulted in better score for the 4-tow case. While this scoring is valid for the given inputs, a further structural analysis examining these defects could be necessary. This analysis would provide a definite answer as to whether the lower defect occurrence with higher severity is a better option than increased defect occurrence with lower severity.

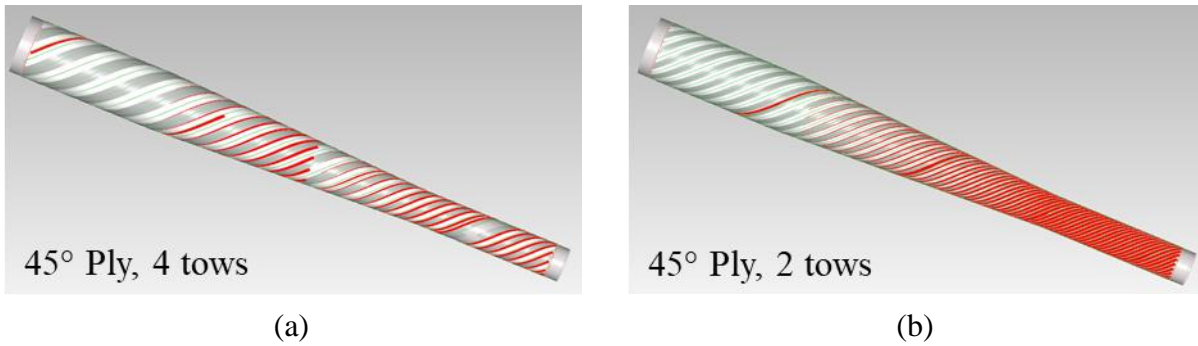


Figure 23: Defect analysis from VCP for 45-degree plies of (a) 4 tow and (b) 2 tow trials

Utilizing the presented results with additional AFP manufacturing knowledge, an optimal strut geometry design can be chosen from the analyzed profiles. From analysis of the scores, the longest transition zone (20 in.) will be the best option. Examining the scores with the individual radii does not show a clear best option. However, it is expected that a smoother transition will result in less defects due to improved roller compression and enhanced transition smoothness. These analyses result in the best geometry being a transition length of 20 in., radii of 2 in., while manufacturing with 4 tows. The selected geometry is shown in Figure 24 below.

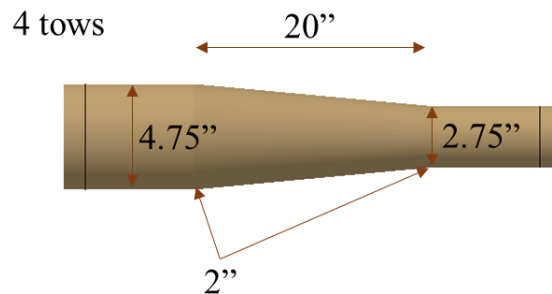


Figure 24: Selected geometry with the overall best results

5. CONCLUSIONS

5.1 Conclusion

The investigations and developments in this study, are vital to the manufacturability of struts through AFP in the future. From the analyses defined in Section 2.1 and 2.2, it was determined a geometry with a diameter of 4.75 in. transitioning over a transition length of 20 in. to a second diameter of 2.75 in and a transition zone initiated and terminated by a smooth transition of a 2 in. radius was the most optimized geometry (Figure 24). It was also found that four tow courses produce less defects than two tow courses during layup. With this information and design tool, the possibility of manufacturing struts through AFP is obtainable.

5.2 Future Work

Future work that needs to be conducted on this topic includes a closed loop composite product lifecycle management (PLM) tool as shown in Figure 25. Where, design, process planning, manufacturing, and post-manufacturing are used in unison to create the most manufacturable strut

design. To increase efficiency in generating new strut geometries it is vital to have an automatic strut creation tool that eliminates the need for a modeling software. Using a system such as PythonOCC, the user could give inputs to create the surface and boundaries and decide on linear or radius geometries. Other improvements consist of surface analysis, that can be used to relate expected/actual defects to surface features and process parameters. The next step is to further develop the design/analysis tool and create a link between process planning data and design variables. Continuous iteration on a single design is assumed to show improvement until some convergence is discovered.

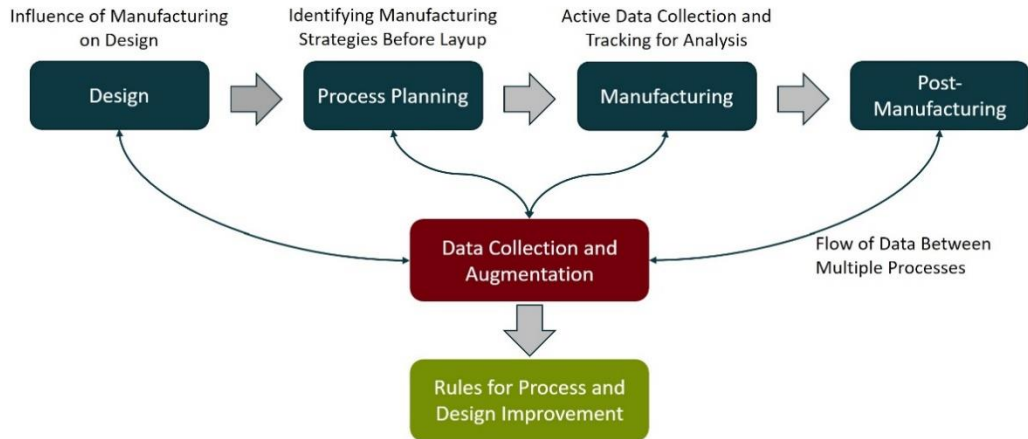


Figure 25: Closed loop composite product lifecycle management tool

6. REFERENCES

- [1] D. Jegley, K. Wu, J. Phelps, M. McKenney and L. Oremont, "Structural Efficiency of Composite Struts for Aerospace Applications," *Journal of Spacecraft and Rockets*, vol. 49, no. 5, pp. 915-924, 2012.
- [2] NASA, "More Abot the Human Landing System Program," 22 Sep 2020. [Online]. Available: <https://www.nasa.gov/content/more-about-the-human-landing-system-program>. [Accessed 2021].
- [3] J. Brewster, "Design of Structurally Efficient Tapered Struts," NASA CR 2009-8393, 2009.
- [4] R. Messinger, "Design of Structurally Efficient Tapered Struts," NASA CR 2010-216698, 2010.
- [5] R. Deo, H. Benner, V. Dawson, E. Olason and R. Harrison, "Design of Structurally Effiecient Tapered Struts (SETS)," NASA CR 2010-216699, 2010.

- [6] N. Bakhshi and M. Hojjati, "An Experimental and Simulative Study on the Defects Appeared During Tow Steering in Automated Fiber Placement," *Composites Part A: Applied Science and Manufacturing*, vol. 113, no. March, 2018.
- [7] R. Wehbe, R. Harik and Z. Gürdal, "In-Plane Tow Deformations due to Steering in Automated Fiber Placement," *AIAA Scitech 2019 Forum*, pp. 1-13, 2019.
- [8] R. Harik, C. Saidu, S. Williams, Z. Gurdal and B. Grimsley, "Automated Fiber Placement Defect Identity Cards: Cause, Anticipation, Existence, Significance, and Progression," *International SAMPE Technical Conference*, Vols. 2018-May, no. September, 2018.
- [9] F. Heinecke and C. Willberg, "Manufacturing-Induced Imperfections in Composite Parts Manufactured via Automated Fiber Placement," *Journal of Composites Science*, vol. 3, no. 2, p. 56, 2019.
- [10] K. Croft, L. Lessard, D. Pasini, M. Hojjati, J. Chen and A. Yousefpour, "Experimental Study of the Effect of Automated Fiber Placement Induced Defects on Performance of Composite Laminates," *Composites Part A: Applied Science and Manufacturing*, vol. 42, no. 5, pp. 484-491, 2011.
- [11] P. Chevalier, C. Kassapoglou and Z. Gürdal, "Fatigue Behavior of Composite Laminates with Automated Fiber Placement Induced Defects- A Review," *International Journal of Fatigue*, vol. 140, no. April, 2020.
- [12] MATLAB, version 9.6.0, Natick, Massachusetts: The Mathworks Inc., 2021.
- [13] "Python Programming Language, version 3.7," Python Software Foundation, [Online]. Available: <https://www.python.org/>.
- [14] M. Jiang, B. Wu and F. Li, "Path Optimization for Open-Contoured Structures in Robotic Fibre Placement," *Proceedings - 2017 32nd Youth Academic Annual Conference of Chinese Association of Automation*, pp. 207-212, 2017.
- [15] L. Li, D. Xu, X. Wang and M. Tan, "A Survey on Path Planning Algorithms in Robotic Fibre Placement," *Proceedings of the 2015 27th Chinese Control and Decision Conference, CCDC 2015*, no. 4, pp. 4704-4709, 2015.
- [16] C. Pupo, "Continuous Tow Path Generation for Constant and Variable Stiffness Composite Laminates on Single and Double Curved Surfaces," *University of South Carolina Scholar Commons*, 2019.
- [17] J. Halbritter, "Automation of Process Planning for Automated Fiber Placement. (Master's Thesis)," 2020. [Online]. Available: <https://scholarcommons.sc.edu/etd/5953/>.

- [18] "VERICUT Composite Programming," CGTech, [Online]. Available: <https://www.cgtech.com/products/vcp.html>. [Accessed 10 2 2021].
- [19] T. Paviot, "PythonOCC," 2021. [Online]. Available: <https://github.com/tpaviot/pythonocc>.